CHALMERS | GÖTEBORGS UNIVERSITET

PREPRINT

Using QR Factorization and SVD to Solve Input Estimation Problems in Structural Dynamics

T PATRIK NORDBERG
IVAR GUSTAFSSON

Department of Mathematics
CHALMERS UNIVERSITY OF TECHNOLOGY
GÖTEBORG UNIVERSITY
Göteborg Sweden 2004

Preprint 2004:37

Using QR Factorization and SVD to Solve Input Estimation Problems in Structural Dynamics

T Patrik Nordberg
Ivar Gustafsson

Mathematics
Department of Mathematics
Chalmers University of Technology and Göteborg University
SE-412 96 Göteborg, Sweden
Göteborg, June 2004

NO 2004:37
ISSN 0347-2809

Matematiska Vetenskaper
Göteborg 2004

Using QR factorization and SVD to Solve Input Estimation Problems in Structural Dynamics

T Patrik Nordberg[⋆] and Ivar Gustafsson[⋆⋆]

[⋆] *Volvo Car Corporation and Department of Applied Mechanics, Chalmers University of Technology, SE-412 96 Göteborg, Sweden.*
patrik.nordberg@me.chalmers.se
[⋆⋆] *Numerical Analysis Group, Department of Mathematics Chalmers University of Technology and Göteborg University.*
ivar@math.chalmers.se

ABSTRACT

Input estimation problems in structural mechanics are in general ill-posed. Treatment of these problems requires that the problems are reformulated, usually by numerical regularization techniques. Several methods of solving input estimation problems, which take the form of structured block matrix problems, are studied in this paper. The investigated methods are based on forming the normal equations, QR factorization and singular value decomposition. A specific block QR factorization algorithm utilizing the structure of the associated upper triangular block Toeplitz matrix is also introduced. Moreover, a criterion for choosing the level of regularization based on the data used to construct L-curves is suggested. Numerical examples are given to illustrate various numerical aspects of the different methods and the performance of the advocated criterion.

1 INTRODUCTION

In structural dynamics, forces acting on a physical structure can be difficult to measure directly. The structure may prohibit the use of a force transducer without it being destroyed or the transducer itself may alter the system properties. In these situations, indirect force measurement techniques must be used. The associated input estimation problem constitutes estimation of the magnitudes of unknown inputs (forces) often using only a fraction of the potentially measurable response data (e.g. accelerations). The spatial distribution of the inputs and the underlying mathematical model of the system are assumed to be known *a priori*.

Reviews of different input estimation methods applied to mechanical dynamic systems can be found in [1], [2] and [3]. Input estimation methods in structural dynamics

are often developed with a specific engineering application in mind; docking forces between two spacecraft [4], reconstruction of forces due to missile impacts [5] and estimation of road profiles for ground excited vehicles [6], to mention just a few. The methods enable the mechanical system to become its own force transducer. Naturally, the practical implications of such methods are truly diverse.

Input estimation problems are in general ill-posed [7], which implies that they need to be reformulated if practically useful solutions are sought. Different regularization techniques are often adopted to reformulate the problem and thereby provide sensible estimates of the unknown inputs, see e.g. [8], [9], [10], [11], [12] and [13]. From the governing equations considered in this paper, a problem formulation incorporating an upper block triangular Toeplitz matrix can be derived. For a survey on techniques for solving systems with Toeplitz matrices see [14] and the references therein, cf also [15]. Moreover, an extensive tutorial survey of numerical algorithms associated with the resulting discrete regularized deconvolution problems is given in [16], cf also [17]. The main purpose of this paper is to investigate and clarify some numerical properties, rendering from the governing equations of mechanical dynamic systems, of principally four different input estimation methods. Furthermore, a criterion for choosing an appropriate level of regularization for this class of problem is suggested.

2 TECHNICAL PRELIMINARIES

Consider a class of linear, causal and time-invariant dynamic systems defined by the following discrete-time state-space equation with n_s states and n_i inputs

$$\boldsymbol{x}_{k+1} = \boldsymbol{A}\boldsymbol{x}_k + \boldsymbol{B}\boldsymbol{u}_k \tag{1}$$

Here, $\boldsymbol{x}_k \in \mathbb{R}^{n_\mathrm{s}}$ and $\boldsymbol{u}_k \in \mathbb{R}^{n_\mathrm{i}}$ are vectors containing states and force inputs, respectively. $\boldsymbol{A}$ denotes the plant matrix and $\boldsymbol{B}$ the input influence matrix. The corresponding discrete-time output equation, with n_o outputs, is given by

$$\boldsymbol{y}_k = \boldsymbol{C}\boldsymbol{x}_k + \boldsymbol{D}\boldsymbol{u}_k \tag{2}$$

where $\boldsymbol{y}_k \in \mathbb{R}^{n_\mathrm{o}}$ is a vector containing the outputs of measurement devices. $\boldsymbol{C}$ and $\boldsymbol{D}$ denote the output influence matrix and the direct throughput matrix, respectively. For a known input sequence $\boldsymbol{u} \stackrel{\text{def}}{=} [\boldsymbol{u}_N^\mathrm{T}\ \boldsymbol{u}_{N-1}^\mathrm{T}\ \ldots\ \boldsymbol{u}_0^\mathrm{T}]^\mathrm{T}$ and known initial states $\boldsymbol{x}_0$ at time $k = 0$, the output relation can be rewritten as

$$\boldsymbol{y}_k = \boldsymbol{C}\boldsymbol{A}^k\boldsymbol{x}_0 + \boldsymbol{D}\boldsymbol{u}_k + \sum_{i=0}^{k-1} \boldsymbol{C}\boldsymbol{A}^i\boldsymbol{B}\boldsymbol{u}_{k-1-i} \tag{3}$$

utilizing Eqs. (1) and (2) for times $k = 0, \ldots, N$, with the definition $\sum_{i=0}^{-1} \ \ldots \stackrel{\text{def}}{=} \boldsymbol{0}$. Furthermore, introducing the *Markov* (impulse response) parameters $\boldsymbol{H}_i \in \mathbb{R}^{n_\text{o} \times n_\text{i}}$ and $\boldsymbol{H}_i^0 \in \mathbb{R}^{n_\text{o} \times n_\text{s}}$

$$\boldsymbol{H}_i \stackrel{\text{def}}{=} \begin{cases} \boldsymbol{D} & i = 0 \\ \boldsymbol{C}\boldsymbol{A}^{i-1}\boldsymbol{B} & i = 1, \ldots, N \end{cases} \tag{4}$$

$$\boldsymbol{H}_i^0 \stackrel{\text{def}}{=} \boldsymbol{C}\boldsymbol{A}^i \qquad i = 0, \ldots, N \tag{5}$$

Eq. (3) can be written in the form

$$\boldsymbol{y}_k = \boldsymbol{H}_k^0 \boldsymbol{x}_0 + \sum_{i=0}^{k} \boldsymbol{H}_i \boldsymbol{u}_{k-i} \tag{6}$$

where $\boldsymbol{H}_k^0$ represents the influence from initial conditions $\boldsymbol{x}_0$ on the output at time step k. The output of the system for a given input can be solved in a straightforward manner if the parameters $\boldsymbol{H}_k^0$ and $\boldsymbol{H}_i$ are known (from analysis or experiments) for all time steps. This is also known as the *direct* or *forward* problem.

Equation (6) can be re-arranged as

$$\boldsymbol{y}_k^0 \stackrel{\text{def}}{=} \boldsymbol{y}_k - \boldsymbol{H}_k^0 \boldsymbol{x}_0 = \sum_{i=0}^{k} \boldsymbol{H}_i \boldsymbol{u}_{k-i} \tag{7}$$

where $\boldsymbol{y}_k^0$ is the output at time k, which has been compensated for effects of non-zero initial conditions. Expressing this relation for each discrete time $k = 0, \ldots, N$ in block matrix form yields

$$\underbrace{\begin{bmatrix} \boldsymbol{H}_0 & \boldsymbol{H}_1 & \ldots & \boldsymbol{H}_N \\ \boldsymbol{0} & \boldsymbol{H}_0 & \ldots & \boldsymbol{H}_{N-1} \\ \vdots & \vdots & \ddots & \vdots \\ \boldsymbol{0} & \boldsymbol{0} & \ldots & \boldsymbol{H}_0 \end{bmatrix}}_{\stackrel{\text{def}}{=} \overline{\boldsymbol{H}}_0} \begin{bmatrix} \boldsymbol{u}_N \\ \boldsymbol{u}_{N-1} \\ \vdots \\ \boldsymbol{u}_0 \end{bmatrix} = \begin{bmatrix} \boldsymbol{y}_N^0 \\ \boldsymbol{y}_{N-1}^0 \\ \vdots \\ \boldsymbol{y}_0^0 \end{bmatrix} \tag{8}$$

It is clear from Eq. (8) that the coefficient matrix $\overline{\boldsymbol{H}}_0$ is in upper block triangular Toeplitz form. This characteristic structure is utilized in Section 3.2. For further treatment of basic linear system theory, cf [18].

3 INPUT ESTIMATION PROBLEM

The *inverse* or *input estimation* problem constitutes computation of the input sequence $\boldsymbol{u}$ for a known sequence of measurements $\hat{\boldsymbol{y}} \stackrel{\text{def}}{=} [\hat{\boldsymbol{y}}_N^\text{T} \ \hat{\boldsymbol{y}}_{N-1}^\text{T} \ \ldots \ \hat{\boldsymbol{y}}_0^\text{T}]^\text{T}$ compensated for effects of non-zero initial conditions $\hat{\boldsymbol{y}}^0 \stackrel{\text{def}}{=} [(\hat{\boldsymbol{y}}_N^0)^\text{T} \ (\hat{\boldsymbol{y}}_{N-1}^0)^\text{T} \ \ldots \ (\hat{\boldsymbol{y}}_0^0)^\text{T}]^\text{T} \stackrel{\text{def}}{=} \hat{\boldsymbol{y}} - [(\boldsymbol{H}_N^0 \boldsymbol{x}_0)^\text{T} \ (\boldsymbol{H}_{N-1}^0 \boldsymbol{x}_0)^\text{T} \ \ldots \ (\boldsymbol{H}_0^0 \boldsymbol{x}_0)^\text{T}]^\text{T}$ of the outputs. The corresponding least squares problem is formulated according to

$$\min_{\boldsymbol{u}} \|\overline{\boldsymbol{H}}_0 \boldsymbol{u} - \hat{\boldsymbol{y}}^0\|_2^2 \tag{9}$$

with the straightforward solution

$$\boldsymbol{u}^\text{LS} = \overline{\boldsymbol{H}}_0^+ \hat{\boldsymbol{y}}^0 \tag{10}$$

where $\overline{\boldsymbol{H}}_0^+ \stackrel{\text{def}}{=} [\overline{\boldsymbol{H}}_0^\text{T} \overline{\boldsymbol{H}}_0]^{-1} \overline{\boldsymbol{H}}_0^\text{T}$ denotes the Moore-Penrose pseudoinverse of $\overline{\boldsymbol{H}}_0$ if $\overline{\boldsymbol{H}}_0$ has full rank. If the number of measured outputs coincide with the number of independent inputs to be identified, i.e. n_o=n_i, $\overline{\boldsymbol{H}}_0$ will be a square matrix and $\overline{\boldsymbol{H}}_0^+$ becomes the regular matrix inverse $\overline{\boldsymbol{H}}_0^{-1}$. Moreover, $\overline{\boldsymbol{H}}_0^{-1}$ then retains the same upper block triangular Toeplitz matrix structure as $\overline{\boldsymbol{H}}_0$ which implies that this particular inverse case is causal. The $N+1$ possibly unique block elements of $\overline{\boldsymbol{H}}_0^{-1}$ can readily be derived explicitly in state-space form or Markov parameter form. The existence of a unique solution requires that the block diagonal element $\boldsymbol{H}_0$ in $\overline{\boldsymbol{H}}_0$ must be of full column rank, which is normally the case for the so-called *collocated* input/output configuration; all inputs have instant and distinguishable influence on the outputs. In general, in case $\boldsymbol{H}_0$ is of full column rank then the entire block matrix $\overline{\boldsymbol{H}}_0$ is of full column rank and there must be at least as many equations as there are unknowns, i.e. $n_\text{o} \geq n_\text{i}$. It should be noted that $\boldsymbol{H}_0$ and therefor also $\overline{\boldsymbol{H}}_0$ is rank deficient if at least one of the inputs lacks instant influence on any of the outputs, the so-called *non-collocated* input/output configuration. Both configurations are studied in this paper.

Equation (9) represents a discretized ill-posed problem since it stems from a convolution integral equation of the first kind, see e.g. [16]. In the discretized case, this is noticed by the gradual decay to zero of the singular values of the coefficient matrix $\overline{\boldsymbol{H}}_0$. But even if the rank deficiency of $\overline{\boldsymbol{H}}_0$ is removed, e.g. by truncation, $\overline{\boldsymbol{H}}_0$ may still be ill-conditioned, i.e. small changes (noise) in the outputs may correspond to large changes in the predicted inputs, which is especially a problem for the non-collocated input/output configuration. Furthermore, the condition number of $\overline{\boldsymbol{H}}_0$ grows as its size increases, i.e. as the number of time steps N increases. Thus, also for long time series, $\overline{\boldsymbol{H}}_0$ may become ill-conditioned. The difficulties associated with a large condition number of $\overline{\boldsymbol{H}}_0$ will in general make any attempt to solve Eq. (9) with Eq. (10) meaningless. In an important class of methods the coefficient matrix is modified, either by regularization or by truncating some expansion of it. These methods incorporate additional information of the sought solution, i.e. place restrictions on $\boldsymbol{u}$. The resulting more well-conditioned problem can then be solved. However, it should be kept in mind

that the error $\delta\boldsymbol{u}$ in the computed solution, regardless of algorithm, is bounded by

$$\frac{\|\delta\boldsymbol{u}\|}{\|\boldsymbol{u}\|} \leq \kappa(\overline{\boldsymbol{H}}_0)\frac{1}{\cos(\theta)}\frac{\|\delta\boldsymbol{y}^0\|}{\|\boldsymbol{y}^0\|}, \qquad \cos(\theta) \stackrel{\text{def}}{=} \frac{\|\overline{\boldsymbol{H}}_0\boldsymbol{u}\|}{\|\hat{\boldsymbol{y}}^0\|} \tag{11}$$

since only output error $\delta\boldsymbol{y}^0 = \hat{\boldsymbol{y}}^0 - \boldsymbol{y}^0$ is considered in this paper, e.g. see [14]. θ is the angle between the vectors $\hat{\boldsymbol{y}}^0$ and $\overline{\boldsymbol{H}}_0\boldsymbol{u}$. Observe that if the residual $\hat{\boldsymbol{y}}^0 - \overline{\boldsymbol{H}}_0\boldsymbol{u}$ is small then $\cos(\theta) \approx 1$. $\kappa(\overline{\boldsymbol{H}}_0)$ denotes the condition number of $\overline{\boldsymbol{H}}_0$. For example, if the relative vector norm output error is $\|\delta\boldsymbol{y}^0\|/\|\boldsymbol{y}^0\| = 1/\kappa(\overline{\boldsymbol{H}}_0)$ and $\cos(\theta) \approx 1$ then the vector norm error in the computed solution may be as large as the solution itself. But for moderate levels of output error compared to the condition number, the methods of modifying $\overline{\boldsymbol{H}}_0$ usually reduce the perturbation error given by Eq. (11). This is illustrated by a numerical example in Section 5.2.

Tikhonov regularization, also known as *damped least squares*, was developed independently by Phillips [8] and Tikhonov [9]. The restrictions on $\boldsymbol{u}$ are imposed by an *a priori* bound on $\|\boldsymbol{L}_i\boldsymbol{u}\|_2$ modifying Eq. (9) to

$$\min_{\boldsymbol{u}}\{\|\overline{\boldsymbol{H}}_0\boldsymbol{u} - \hat{\boldsymbol{y}}^0\|_2^2 + \lambda\|\boldsymbol{L}_i\boldsymbol{u}\|_2^2\} \tag{12}$$

where $\lambda \in [0, \infty)$ is the regularization parameter that controls the balance between the restrictions on $\boldsymbol{u}$ and the minimization of the residual norm. A method for choosing a specific λ accommodating for this balance is discussed in Section 4. $\boldsymbol{L}_i \in \mathbb{R}^{n_{\mathrm{L}} \times n_{\mathrm{i}}(N+1)}$, where $n_{\mathrm{L}} \leq n_{\mathrm{i}}(N+1)$, is typically a discrete approximation to the ith-order derivative operator. For example, *zeroth-order* Tikhonov regularization corresponds to choosing $\boldsymbol{L}_0 = \boldsymbol{I} \in \mathbb{R}^{n_{\mathrm{i}}(N+1) \times n_{\mathrm{i}}(N+1)}$ and *first-order* Tikhonov regularization corresponds to choosing

$$\boldsymbol{L}_1 = \begin{bmatrix} \boldsymbol{I} & -\boldsymbol{I} & \boldsymbol{0} & \dots & \boldsymbol{0} \\ \boldsymbol{0} & \boldsymbol{I} & -\boldsymbol{I} & \dots & \boldsymbol{0} \\ \vdots & \vdots & \ddots & \ddots & \vdots \\ \boldsymbol{0} & \boldsymbol{0} & \dots & \boldsymbol{I} & -\boldsymbol{I} \end{bmatrix} \in \mathbb{R}^{n_{\mathrm{i}}N \times n_{\mathrm{i}}(N+1)}, \qquad \boldsymbol{I} \in \mathbb{R}^{n_{\mathrm{i}} \times n_{\mathrm{i}}}$$

except for a scaling factor. The formulation of the damped least squares problem given by Eq. (12) is not well suited for numerical computation but it is equivalent to an expanded or enlarged formulation given as

$$\min_{\boldsymbol{u}} \left\| \begin{bmatrix} \overline{\boldsymbol{H}}_0 \\ \sqrt{\lambda}\boldsymbol{L}_i \end{bmatrix} \boldsymbol{u} - \begin{bmatrix} \hat{\boldsymbol{y}}^0 \\ \boldsymbol{0} \end{bmatrix} \right\|_2 \tag{13}$$

The solution to Eq. (13) may be formed in numerous ways, e.g. by use of QR factorization, (truncated) singular value decomposition, or computation of an inverse matrix by forming the corresponding normal equations, cf [19], [17], [13], [20], and [16].

The method of normal equations is a classical way of solving damped least squares

problems dating back to Gauss. Applying the method to Eq. (13) yields

$$(\overline{\boldsymbol{H}}_0^{\mathrm{T}}\overline{\boldsymbol{H}}_0 + \lambda\boldsymbol{L}_i^{\mathrm{T}}\boldsymbol{L}_i)\boldsymbol{u}^{\mathrm{NE}} = \overline{\boldsymbol{H}}_0^{\mathrm{T}}\hat{\boldsymbol{y}}^0 \tag{14}$$

where $\overline{\boldsymbol{H}}_0^{\mathrm{T}}\overline{\boldsymbol{H}}_0 + \lambda\boldsymbol{L}_i^{\mathrm{T}}\boldsymbol{L}_i$ is symmetric and positive definite if $\lambda > 0$. A unique regularized solution $\boldsymbol{u}^{\mathrm{NE}}$ to Eq. (14) is computed as

$$\boldsymbol{u}^{\mathrm{NE}} = (\overline{\boldsymbol{H}}_0^{\mathrm{T}}\overline{\boldsymbol{H}}_0 + \lambda\boldsymbol{L}_i^{\mathrm{T}}\boldsymbol{L}_i)^{-1}\overline{\boldsymbol{H}}_0^{\mathrm{T}}\hat{\boldsymbol{y}}^0 \tag{15}$$

for a given λ. The major drawback in forming and solving the normal equations is that significant information may by lost since the condition number of $\overline{\boldsymbol{H}}_0^{\mathrm{T}}\overline{\boldsymbol{H}}_0$ is the condition number of $\overline{\boldsymbol{H}}_0$ squared, i.e. for small values of λ, $\overline{\boldsymbol{H}}_0^{\mathrm{T}}\overline{\boldsymbol{H}}_0 + \lambda\boldsymbol{L}_i^{\mathrm{T}}\boldsymbol{L}_i$ may be ill-conditioned and serious loss of accuracy in the computed solution may occur. This will be illustrated in the succeeding numerical examples. It should be noted that the input estimation problem is non-causal if $n_{\mathrm{o}} > n_{\mathrm{i}}$ and/or $\lambda > 0$.

The theory of four principally different methods for solving the input estimation problem is given next. Three of the methods are based on QR factorization and the remaining method on singular value decomposition (SVD). Numerical aspects of these methods and the solution corresponding to the normal equations, Eq. (15), are investigated in Section 5.

3.1 QR factorization

QR factorization is a representation of a matrix in simpler form via orthogonal transformations. Because of the excellent numerical properties associated with QR factorization, it is frequently applied to linear least squares problems, e.g. see [14]. Consider the expanded formulation of the damped least squares problem given by Eq. (13) and let $\boldsymbol{Q} \in \mathbb{R}^{n_{\mathrm{o}}(N+1)+n_{\mathrm{L}} \times n_{\mathrm{o}}(N+1)+n_{\mathrm{L}}}$ be an orthogonal matrix, i.e. $\boldsymbol{Q}^{\mathrm{T}}\boldsymbol{Q} = \boldsymbol{I}$. Since orthogonal transformations preserve the Euclidian length, Eq. (13) is equivalent to

$$\min_{\boldsymbol{u}} \left\| \boldsymbol{Q}^{\mathrm{T}} \left(\begin{bmatrix} \overline{\boldsymbol{H}}_0 \\ \sqrt{\lambda}\boldsymbol{L}_i \end{bmatrix} \boldsymbol{u} - \begin{bmatrix} \hat{\boldsymbol{y}}^0 \\ \boldsymbol{0} \end{bmatrix} \right) \right\|_2 \tag{16}$$

The QR factorization

$$\begin{bmatrix} \overline{\boldsymbol{H}}_0 \\ \sqrt{\lambda}\boldsymbol{L}_i \end{bmatrix} = \boldsymbol{Q} \begin{bmatrix} \boldsymbol{R} \\ \boldsymbol{0} \end{bmatrix} \tag{17}$$

is formed by multiplications of successive Householder transformations. The *R-factor* or $\boldsymbol{R} \in \mathbb{R}^{n_{\mathrm{i}}(N+1) \times n_{\mathrm{i}}(N+1)}$ is upper triangular and nonsingular. Inserting Eq. (17) into Eq. (16) yields

$$\min_{\boldsymbol{u}} \left\| \begin{bmatrix} \boldsymbol{R} \\ \boldsymbol{0} \end{bmatrix} \boldsymbol{u} - \boldsymbol{Q}^{\mathrm{T}} \begin{bmatrix} \hat{\boldsymbol{y}}^0 \\ \boldsymbol{0} \end{bmatrix} \right\|_2 \tag{18}$$

By partitioning $\boldsymbol{Q}$ according to

$$\boldsymbol{Q} \stackrel{\text{def}}{=} \left[\begin{array}{c|c} \boldsymbol{Q}_{11} & \\ \boldsymbol{Q}_{12} & \boldsymbol{Q}_2 \end{array}\right] \tag{19}$$

where $\boldsymbol{Q}_{11} \in \mathbb{R}^{n_{\text{o}}(N+1)\times n_{\text{i}}(N+1)}$, it is possible to rewrite Eq. (18) as

$$\min_{\boldsymbol{u}}\{\|\boldsymbol{R}\boldsymbol{u} - \boldsymbol{Q}_{11}^{\text{T}}\hat{\boldsymbol{y}}^0\|_2^2 + \|\boldsymbol{Q}_2^{\text{T}}\left[\,(\hat{\boldsymbol{y}}^0)^{\text{T}}\;\;\boldsymbol{0}^{\text{T}}\,\right]^{\text{T}}\|_2^2\} \tag{20}$$

The minimum is clearly defined by the upper triangular system

$$\boldsymbol{R}\boldsymbol{u} = \boldsymbol{Q}_{11}^{\text{T}}\hat{\boldsymbol{y}}^0 \tag{21}$$

which is usually solved by back-substitution. For notational purposes, the solution corresponding to Eq. (21) is given as

$$\boldsymbol{u}^{\text{QR}} \stackrel{\text{def}}{=} \boldsymbol{R}^{-1}\boldsymbol{Q}_{11}^{\text{T}}\hat{\boldsymbol{y}}^0 \tag{22}$$

It should be noted that the entire $\boldsymbol{Q}$-matrix does not need to be formed. It is sufficient to compute the left block column of $\boldsymbol{Q}$ as given by Eq. (19) and the R-factor, yielding

$$\begin{bmatrix} \overline{\boldsymbol{H}}_0 \\ \sqrt{\lambda}\boldsymbol{L}_i \end{bmatrix} = \begin{bmatrix} \boldsymbol{Q}_{11} \\ \boldsymbol{Q}_{12} \end{bmatrix} \boldsymbol{R} \tag{23}$$

which is called *compact* QR factorization.

3.2 Block QR factorization

In this section, the block structure of the coefficient matrix is utilized to present an algorithm based on QR factorization, called *block QR factorization*. Block algorithms are often developed to achieve high computational performance, and the principles for such algorithms can be found in [17] and references therein. Consider the compact QR factorization of the expanded coefficient matrix in Eq. (13) with $\boldsymbol{L}_i = \boldsymbol{L}_0$, i.e. zeroth-order Tikhonov regularization,

$$\begin{bmatrix} \overline{\boldsymbol{H}}_0 \\ \sqrt{\lambda}\boldsymbol{I} \end{bmatrix} = \overline{\boldsymbol{Q}}\,\overline{\boldsymbol{R}} \tag{24}$$

The expanded coefficient matrix consists of $N+1$ blocks of columns. It is possible, e.g. cf [17] for general block matrix structures, to construct a compact QR factorization on

a block-to-block basis by defining $\overline{\boldsymbol{Q}}$ according to

$$\overline{\boldsymbol{Q}} \stackrel{\text{def}}{=} \begin{bmatrix} \boldsymbol{Q}_0^{(1)} & \boldsymbol{Q}_1^{(1)} & \dots & \boldsymbol{Q}_{N-1}^{(1)} & \boldsymbol{Q}_N \\ \boldsymbol{0} & & & & \\ \boldsymbol{0} & \boldsymbol{0} & & & \\ \vdots & \vdots & \ddots & & \\ \boldsymbol{0} & \boldsymbol{0} & \dots & \boldsymbol{0} & \\ \boldsymbol{Q}_0^{(2)} & \boldsymbol{Q}_1^{(2)} & \dots & \boldsymbol{Q}_{N-1}^{(2)} & \\ \boldsymbol{0} & & & & \\ \boldsymbol{0} & \boldsymbol{0} & & & \\ \vdots & \vdots & \ddots & & \\ \boldsymbol{0} & \boldsymbol{0} & \dots & \boldsymbol{0} & \end{bmatrix} \tag{25}$$

where $\overline{\boldsymbol{Q}} \in \mathbb{R}^{(n_{\text{o}}+n_{\text{i}})(N+1)\times n_{\text{i}}(N+1)}$, $\boldsymbol{Q}_N \in \mathbb{R}^{(n_{\text{o}}+n_{\text{i}})(N+1)\times n_{\text{i}}}$ and $\boldsymbol{Q}_p^{(1)} \in \mathbb{R}^{n_{\text{o}}(p+1)\times n_{\text{i}}}$, $\boldsymbol{Q}_p^{(2)} \in \mathbb{R}^{n_{\text{i}}(p+1)\times n_{\text{i}}}$ for $p = 0, 1, \dots, N-1$. Moreover, $\overline{\boldsymbol{R}}$ is defined by

$$\overline{\boldsymbol{R}} \stackrel{\text{def}}{=} \begin{bmatrix} \overline{\boldsymbol{R}}_{0,0} & \overline{\boldsymbol{R}}_{0,1} & \dots & \overline{\boldsymbol{R}}_{0,N} \\ \boldsymbol{0} & \overline{\boldsymbol{R}}_{1,1} & \dots & \overline{\boldsymbol{R}}_{1,N} \\ \vdots & \vdots & \ddots & \vdots \\ \boldsymbol{0} & \boldsymbol{0} & \dots & \overline{\boldsymbol{R}}_{N,N} \end{bmatrix} \tag{26}$$

which is upper block triangular with elements $\overline{\boldsymbol{R}}_{i,j} \in \mathbb{R}^{n_{\text{i}}\times n_{\text{i}}}$ according to

$$\overline{\boldsymbol{R}}_{i,j} \stackrel{\text{def}}{=} \begin{cases} \boldsymbol{R}_i & i = j \\ (\boldsymbol{Q}_i^{(1)})^{\text{T}}\begin{bmatrix} \boldsymbol{H}_j^{\text{T}} & \boldsymbol{H}_{j-1}^{\text{T}} & \dots & \boldsymbol{H}_{j-i}^{\text{T}} \end{bmatrix}^{\text{T}} & i < j \end{cases} \tag{27}$$

for $i = 0, 1, \dots, j$ and $j = 0, 1, \dots, N$. $\boldsymbol{R}_i$ is upper triangular and nonsingular, cf Eqs. (28), (30) and (31). It should be stressed that the matrix

$$\begin{bmatrix} \boldsymbol{H}_j^{\text{T}} & \boldsymbol{H}_{j-1}^{\text{T}} & \dots & \boldsymbol{H}_{j-i}^{\text{T}} \end{bmatrix}^{\text{T}}$$

given in Eq. (27) consists of decreasing indices only, i.e. if $i = 1$ and $j = 3$ the matrix is given by $\begin{bmatrix} \boldsymbol{H}_3^{\text{T}} & \boldsymbol{H}_2^{\text{T}} \end{bmatrix}^{\text{T}}$. Using Eqs. (24)–(27) the compact QR factorization of the first block column of the expanded coefficient matrix is

$$\begin{bmatrix} \boldsymbol{H}_0 \\ \sqrt{\lambda}\boldsymbol{I} \end{bmatrix} = \begin{bmatrix} \boldsymbol{Q}_0^{(1)} \\ \boldsymbol{Q}_0^{(2)} \end{bmatrix} \boldsymbol{R}_0 \tag{28}$$

which is computed by multiplications of successive Householder transformations. Note that only nonzero block rows are utilized in forming Eq. (28). Proceeding to the second

block column yields

$$\begin{bmatrix} \boldsymbol{H}_1 \\ \boldsymbol{H}_0 \\ \boldsymbol{0} \\ \sqrt{\lambda}\boldsymbol{I} \end{bmatrix} = \begin{bmatrix} \boldsymbol{Q}_1^{(1)} \\ \boldsymbol{Q}_1^{(2)} \end{bmatrix} \boldsymbol{R}_1 + \begin{bmatrix} \boldsymbol{Q}_0^{(1)}(\boldsymbol{Q}_0^{(1)})^{\mathrm{T}}\boldsymbol{H}_1 \\ \boldsymbol{0} \\ \boldsymbol{Q}_0^{(2)}(\boldsymbol{Q}_0^{(1)})^{\mathrm{T}}\boldsymbol{H}_1 \\ \boldsymbol{0} \end{bmatrix} \tag{29}$$

Rearranging Eq. (29) yields the compact QR factorization of the second block column as

$$\begin{bmatrix} (\boldsymbol{I} - \boldsymbol{Q}_0^{(1)}(\boldsymbol{Q}_0^{(1)})^{\mathrm{T}})\boldsymbol{H}_1 \\ \boldsymbol{H}_0 \\ -\boldsymbol{Q}_0^{(2)}(\boldsymbol{Q}_0^{(1)})^{\mathrm{T}}\boldsymbol{H}_1 \\ \sqrt{\lambda}\boldsymbol{I} \end{bmatrix} = \begin{bmatrix} \boldsymbol{Q}_1^{(1)} \\ \boldsymbol{Q}_1^{(2)} \end{bmatrix} \boldsymbol{R}_1 \tag{30}$$

Similarly, the compact QR factorization of the third block column is given by

$$\begin{bmatrix} (\boldsymbol{I} - \boldsymbol{Q}_0^{(1)}(\boldsymbol{Q}_0^{(1)})^{\mathrm{T}})\boldsymbol{H}_2 \\ \boldsymbol{H}_1 \\ \boldsymbol{H}_0 \\ -\boldsymbol{Q}_0^{(2)}(\boldsymbol{Q}_0^{(1)})^{\mathrm{T}}\boldsymbol{H}_2 \\ \boldsymbol{0} \\ \sqrt{\lambda}\boldsymbol{I} \end{bmatrix} - \begin{bmatrix} \boldsymbol{Q}_1^{(1)}(\boldsymbol{Q}_1^{(1)})^{\mathrm{T}} \begin{bmatrix} \boldsymbol{H}_2 \\ \boldsymbol{H}_1 \end{bmatrix} \\ \boldsymbol{0} \\ \boldsymbol{Q}_1^{(2)}(\boldsymbol{Q}_1^{(1)})^{\mathrm{T}} \begin{bmatrix} \boldsymbol{H}_2 \\ \boldsymbol{H}_1 \end{bmatrix} \\ \boldsymbol{0} \end{bmatrix} = \begin{bmatrix} \boldsymbol{Q}_2^{(1)} \\ \boldsymbol{Q}_2^{(2)} \end{bmatrix} \boldsymbol{R}_2 \tag{31}$$

The procedure continues for all remaining block columns until the last compact QR factorization, i.e. $\boldsymbol{Q}_N\boldsymbol{R}_N$, is established. This concludes the block algorithm for computing the block elements of $\overline{\boldsymbol{Q}}$ and $\overline{\boldsymbol{R}}$. A block algorithm for first-order Tikhonov regularization can be derived in a similar manner. As in the previous section (compare Eq. (21)), the minimal Euclidian norm solution is defined by the upper triangular system

$$\overline{\boldsymbol{R}}\boldsymbol{u} = \overline{\boldsymbol{Q}}^{\mathrm{T}}\hat{\boldsymbol{y}}^0 \tag{32}$$

which is usually solved by back-substitution. However, the solution is also given as

$$\boldsymbol{u}^{\mathrm{BQR}} \stackrel{\mathrm{def}}{=} \overline{\boldsymbol{R}}^{-1}\overline{\boldsymbol{Q}}^{\mathrm{T}}\hat{\boldsymbol{y}}^0 \tag{33}$$

for notational purposes.

The concept of *flops* is commonly used to quantify the operation counts in numerical algorithms. It can be shown that theoretically, i.e. with optimal implementation, the block QR factorization requires approximately $\mathcal{O}(n_{\mathrm{o}}{n_{\mathrm{i}}}^2(N+1)^2)$ flops. This should be compared with $\mathcal{O}(n_{\mathrm{o}}{n_{\mathrm{i}}}^2(N+1)^3)$ flops for the standard QR factorization given in Section 3.1. Thus, the block factorization is expected to be less expensive, especially for an increasing number of time steps N. However, this factorization is numerically

unstable for large N. These instabilities may be grossly amplified by a large condition number of $\overline{\boldsymbol{Q}}$, which is illustrated by the numerical results given in Section 5.3. It can be shown that $\overline{\boldsymbol{Q}}$ is mathematically orthogonal but numerically, i.e. with finite numerical working precision, there will generally be a gradual loss of orthogonality in the computed block columns of $\overline{\boldsymbol{Q}}$ due to roundoff errors. To ensure the numerical orthogonality of $\overline{\boldsymbol{Q}}$, *reorthogonalization* procedures , cf [17], are often utilized at the expense of an increased operation count. The development of a reorthogonalization procedure for this specific block QR factorization is considered to be beyond the scope of this paper.

3.3 QR factorization with column pivoting

There exists a signal transfer time from at least one input to the measured outputs for the non-collocated input/output configuration. This time delay is studied in detail in [21], cf also [4], [22] and [23], and generally results in a rank deficient coefficient matrix $\overline{\boldsymbol{H}}_0$. In this paper, an alternative method based on QR factorization with *column pivoting* is assessed. QR factorization with column pivoting is a precise way of detecting and dealing with rank deficiency, see e.g. [14] for further details. A numerical example, in which the measurement data is free from noise, is given in Section 5.3.

Consider the coefficient matrix $\overline{\boldsymbol{H}}_0$ for the non-collocated input/output configuration, i.e. $\mathrm{rank}(\overline{\boldsymbol{H}}_0) = r < n_{\mathrm{i}}(N+1)$. QR factorization with column pivoting amounts to selecting a maximal linearly independent subset of $\overline{\boldsymbol{H}}_0$'s columns by repeated column interchanges and orthogonal transformations. This produces the factorization

$$\overline{\boldsymbol{H}}_0\boldsymbol{P} = \boldsymbol{Q}\boldsymbol{R} \stackrel{\mathrm{def}}{=} \boldsymbol{Q} \begin{bmatrix} \boldsymbol{R}_{11} & \boldsymbol{R}_{12} \\ \boldsymbol{0} & \boldsymbol{0} \end{bmatrix} \tag{34}$$

where $\boldsymbol{P}$ is a permutation matrix, $\boldsymbol{Q} \in \mathbb{R}^{n_{\mathrm{o}}(N+1)\times n_{\mathrm{o}}(N+1)}$ is orthogonal, $\boldsymbol{R}_{11} \in \mathbb{R}^{r\times r}$ is upper triangular and nonsingular, and $\boldsymbol{R} \in \mathbb{R}^{n_{\mathrm{o}}(N+1)\times n_{\mathrm{i}}(N+1)}$. In general, the unreduced columns corresponding to the bottom right partition of $\boldsymbol{R}$ will not be exactly zero due to finite numerical precision. This is resolved by monitoring the norm of the partition and terminating the factorization, i.e. setting the partition to zero, when the norm is less than some termination criterion. If $\boldsymbol{R}_{12}$ is set to zero, then it is possible to formulate a *basic solution* to the least squares problem defined by Eq. (9) according to

$$\boldsymbol{u}^{\mathrm{B}} = \boldsymbol{P} \begin{bmatrix} \boldsymbol{R}_{11}^{-1}\boldsymbol{c} \\ \boldsymbol{0} \end{bmatrix} \tag{35}$$

where $\boldsymbol{c}$ is taken as the first r rows of $\boldsymbol{Q}^{\mathrm{T}}\hat{\boldsymbol{y}}^0$. The basic solution has at most r nonzero components but it is not the minimal Euclidian norm solution unless $\boldsymbol{R}_{12}$ is zero.

However, it can be shown that the solution is bounded by

$$1 \leq \frac{\|\boldsymbol{u}^{\mathrm{B}}\|_2}{\|\boldsymbol{u}^{\mathrm{QRLS}}\|_2} \leq \sqrt{1 + \|\boldsymbol{R}_{11}^{-1}\boldsymbol{R}_{12}\|_2^2} \tag{36}$$

where $\boldsymbol{u}^{\mathrm{QRLS}}$ is the minimal Euclidian norm solution, see [14].

3.4 Truncated SVD

Singular value decomposition (SVD) of a matrix is a versatile tool for treating least squares problems, e.g. cf [14]. The SVD of the real-valued coefficient matrix $\overline{\boldsymbol{H}}_0$ takes the form

$$\overline{\boldsymbol{H}}_0 = \boldsymbol{U}\boldsymbol{\Sigma}\boldsymbol{V}^{\mathrm{T}} \tag{37}$$

where $\boldsymbol{U} \in \mathbb{R}^{n_{\mathrm{o}}(N+1)\times n_{\mathrm{o}}(N+1)}$ and $\boldsymbol{V} \in \mathbb{R}^{n_{\mathrm{i}}(N+1)\times n_{\mathrm{i}}(N+1)}$ are orthogonal matrices. $\boldsymbol{\Sigma} \in \mathbb{R}^{n_{\mathrm{o}}(N+1)\times n_{\mathrm{i}}(N+1)}$ is a quasi-diagonal matrix with singular values σ_i as diagonal entries and ordered according to

$$\sigma_1 \geq \sigma_2 \geq \ldots \geq \sigma_{n_{\mathrm{i}}(N+1)} \geq 0$$

The number of non-zero singular values is equal to the rank of $\overline{\boldsymbol{H}}_0$. The minimal Euclidian norm solution to Eq. (9) with a possibly rank deficient $\overline{\boldsymbol{H}}_0$ is given by

$$\boldsymbol{u}^{\mathrm{SVD}} = \boldsymbol{u}^{\mathrm{QRLS}} = \sum_{\sigma_i \neq 0} \frac{\boldsymbol{U}_i^{\mathrm{T}}\hat{\boldsymbol{y}}^0}{\sigma_i}\boldsymbol{V}_i \tag{38}$$

where the column vectors $\boldsymbol{U}_i$ of $\boldsymbol{U}$ and $\boldsymbol{V}_i$ of $\boldsymbol{V}$ are the left and right singular vectors, respectively. By disregarding (truncating) the singular values of $\overline{\boldsymbol{H}}_0$ that are zero in Eq. (38), the rank deficiency is removed. However, the resulting decomposition may still be ill-conditioned, as discussed in Section 3. Equation (38) can be modified to satisfy Eq. (13) with $\boldsymbol{L}_i = \boldsymbol{L}_0$, e.g. see [17]. The modified solution is given as

$$\boldsymbol{u}^{\mathrm{SVDF}} = \sum_{i=1}^{n_{\mathrm{i}}(N+1)} f_i \frac{\boldsymbol{U}_i^{\mathrm{T}}\hat{\boldsymbol{y}}^0}{\sigma_i}\boldsymbol{V}_i \tag{39}$$

where $f_i \stackrel{\mathrm{def}}{=} \sigma_i^2/(\sigma_i^2 + \lambda)$ are the *Tikhonov filter factors*. The filter factors control the damping of the individual singular values of the solution $\boldsymbol{u}^{\mathrm{SVDF}}$, i.e. if $\lambda \ll \sigma_i^2$ then $f_i \approx 1$ or if $\lambda \gg \sigma_i^2$ then $f_i \ll 1$. For moderate values of λ, in a region between the two extremes, the solution will approximately equal the truncated SVD solution

$$\boldsymbol{u}^{\mathrm{TSVD}} = \sum_{i=1}^{k} \frac{\boldsymbol{U}_i^{\mathrm{T}}\hat{\boldsymbol{y}}^0}{\sigma_i}\boldsymbol{V}_i \tag{40}$$

where k is an integer bounded by $1 \leq k < n_{\mathrm{i}}(N+1)$. This decomposition corresponds to the closest matrix of rank k to $\overline{\boldsymbol{H}}_0$, see e.g. [14]. Naturally, an appropriate choice of truncation parameter k is essential. This choice is discussed in Section 4.

4 L-CURVE

A criterion for determining a suitable level of regularization λ and truncation k needs to be established. In this paper, the parameters are chosen by means of the L-curve, the use of which is advocated by Hansen in [11] for discretized ill-posed problems. This curve is used extensively in the proceeding numerical examples to investigate and explain numerical properties of the solutions given by the different methods in Section 3.

The L-curve derives its name from a plot of $(\|\overline{\boldsymbol{H}}_0\boldsymbol{u}^\bullet - \hat{\boldsymbol{y}}^0\|_2, \|\boldsymbol{L}_i\boldsymbol{u}^\bullet\|_2)$ for $\lambda \in [0, \infty)$ (or the truncation parameter k) in a doubly logarithmic scale, which typically forms an L-shaped curve. The superscript $\bullet$ should be replaced by the specific solution being analyzed, i.e. NE, QR, BQR, B or TSVD. Since the true solution $\hat{\boldsymbol{u}}$ is unknown, the optimal regularization (or truncation) parameter minimizing $\|\hat{\boldsymbol{u}} - \boldsymbol{u}^\bullet\|_2$ can generally not be obtained. However, a near optimal parameter can be found in correspondence to the maximum curvature of the "corner" in this graph. Other frequently adopted near optimal criteria amount to choosing the parameter corresponding "slightly" to the right of the "corner". Thus, these criteria produce higher levels of regularization than the criterion based on the maximum curvature.

For the collocated input/output configuration the L-shaped curve will in general not appear, since $\overline{\boldsymbol{H}}_0$ is typically well-conditioned in that case. This implies that neither regularization or truncation is needed to produce a satisfactory solution. However, perturbation errors associated with Eq. (11) may still be present. Thus, it is desirable to use regularization (or truncation) also in this case. A regularization (or truncation) criterion can be established by monitoring the *output residual norm* $\|\overline{\boldsymbol{H}}_0\boldsymbol{u}^\bullet - \hat{\boldsymbol{y}}^0\|_2$ for a decreasing regularization (or increasing truncation) parameter which is sufficiently small and of constant order of magnitude. In general, the output residual norm will decrease for a decreasing regularization (or increasing truncation) parameter and eventually "level off" at a plateau. When the relative difference between two consecutive output residual norms is smaller than some tolerance ϵ_{tol}, the value of the regularization (or truncation) parameter for the largest norm of the two is chosen. The *solution norm* $\|\boldsymbol{L}_i\boldsymbol{u}^\bullet\|_2$ should not be suspiciously large considering the chosen parameter. This is used as a safeguard for numerical errors. This criterion for choosing the regularization (or truncation) parameter is used throughout the numerical examples given next. When the L-shaped curve is present, typically for the non-collocated input/output configuration, the advocated criterion also corresponds to a parameter "slightly" to the right of the "corner".

5 NUMERICAL EXAMPLES

The aim of this section is to illustrate and compare the numerical properties of the preceding methods of solving the input estimation problem in structural dynamics. It is demonstrated how interpretation of the data used to construct L-curves is essential in assessing the validity of the identified inputs.

5.1 Model description and data generation

The model, depicted in Fig. 1, represents a 20 degree-of-freedom mass chain and it is used in the following numerical examples. The spring stiffness is $k = 1$ N/m and all masses are equal; $m_i = 1$ kg for $i = 1, \ldots, 20$. A stiffness-proportional viscous damping with a proportionality constant of 0.1% is added to the model. The resonance frequencies of the system range from $f_{\min} = 0.0122$ Hz to $f_{\max} = 0.317$ Hz. In all examples the system is excited by a transient force (input) applied to mass m_6. The non-zero part of the continuous-time excitation is defined according to

$$\hat{u}_6(t) = (1 - \cos 2\pi f_0 t) \sin 6\pi f_0 t \qquad 0 < t < \frac{1}{f_0} \tag{41}$$

where $f_0 = 0.06$ Hz. All succeeding analyses are carried out for one period of the lowest resonance frequency, i.e. 82 seconds, corresponding to $N + 1 = 501$ time steps using a sampling frequency $f_{\text{samp}} = 6$ Hz. The discrete-time counterpart of the excitation given by Eq. (41) is active for the first 100 time steps. This excitation $\hat{\boldsymbol{u}}$ is shown in Fig. 2.

Measurement acceleration data $\hat{\boldsymbol{y}}^0$ is generated by solving the forward problem described by Eq. (8) and artificially adding noise to the calculated response $\boldsymbol{y}^0$. The input $\boldsymbol{u}$ in Eq. (8) is taken as $\hat{\boldsymbol{u}}$ and the initial states $\boldsymbol{x}_0$ are zero. The fictitious measurement data is established for sensor i and time step $k = 0, \ldots, N$ according to

$$\hat{y}^0_{i,k} = y^0_{i,k}(1 + \epsilon_{\text{noise}}(U(0,1) - 0.5)) \tag{42}$$

i.e. centered uniformly distributed white noise $U(0,1) \in [0,1]$ at a level of ϵ_{noise} relative to each individual value is added to the unperturbed output $\boldsymbol{y}^0$. The input estimation

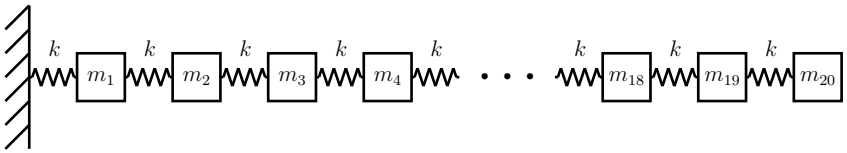

Figure 1: Mass chain with 20 degrees of freedom.

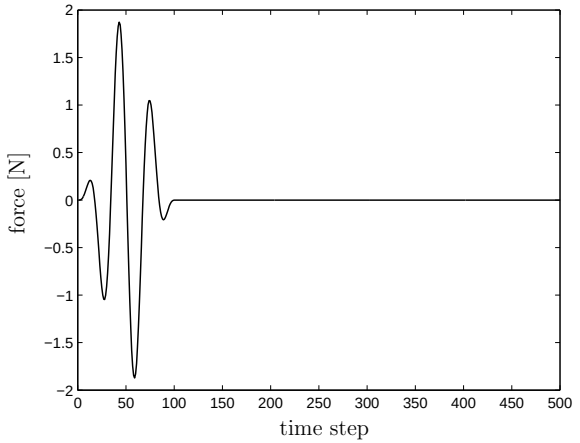

Figure 2: Transient force (input) $\hat{\boldsymbol{u}}$ applied to mass m_6.

is carried out using an otherwise ideal system description. Moreover, the number and positioning of sensors used in the succeeding examples is such that the system is fully observable and controllable. This means that all eigenmodes can be detected and excited by the used sensor/input configuration.

5.2 Collocated input/output configuration

The collocated input/output configuration is an idealized case of theoretical importance rather than of physical importance in structural dynamics. In practice, there will always be a signal transfer time from input to output, i.e. the non-collocated input/output configuration. The purpose of this section is twofold; First, possible effects associated with Eq. (11) are studied by varying the level of noise ϵ_{noise} on the output, cf Eq. (42). Both input estimations corresponding to zeroth-order and first-order Tikhonov regularization are treated. Secondly, the advocated method of choosing a regularization parameter, given in Section 4, is illustrated and it seems to be effective even when the L-curve is not present.

Consider the case of two accelerometers y_6, y_{15} attached to masses m_6 and m_{15}. This is an example of a collocated input/output configuration, since the input (force) is applied to mass m_6. The coefficient matrix is of full rank and well-conditioned, $\kappa(\overline{\boldsymbol{H}}_0) \approx 1.4 \cdot 10^3$ which implies that the pseudo-inverse can be computed within numerical working precision, here $\epsilon_{\text{mach}} \approx 10^{-16}$. Due to this small condition number, the input estimation given by the method of normal equations will be satisfactory.

Thus, only input estimations given by Eq. (15) are studied in this section. In this first numerical example a moderate level of output noise $\epsilon_{\text{noise}} = 10^{-3}$ is added to the unperturbed output according to Eq. (42). Utilizing Eq. (15), input estimations for a decreasing regularization parameter are computed. Typical results for zeroth-order and first-order regularization are given in Tables 1 and 2, respectively. Note that the *solution error norm* $\|\boldsymbol{u}^{\text{NE}} - \hat{\boldsymbol{u}}\|_2$ is not available in practice, since the true solution $\hat{\boldsymbol{u}}$ is unknown. It is used here, to asses the validity of the chosen input estimation. The decrease of the regularization parameter by a constant factor of 10 was found to be an adequate mix between relatively small changes in the output residual norm and the computational expense. Furthermore, the tolerance ϵ_{tol} between two consecutive output residual norms is chosen as $\epsilon_{\text{tol}} = 0.05$. Naturally, the chosen order of decrease of the regularization parameter will affect the chosen tolerance. The output residual norm converges to $\|\hat{\boldsymbol{y}}^0\|_2$ as $\lambda \to \infty$ regardless of input/output configuration and/or regularization method considered in this paper, since $\|\boldsymbol{u}^{\text{NE}}\|_2 \to 0$ when $\lambda \to \infty$. As seen in Tables 1 and 2, the output residual norm decreases as the regularization parameter decreases and eventually "levels off" at a plateau. It has been observed that once the plateau is reached, the output residual norm is relatively insensitive, within an interval, to further changes of the regularization parameter, especially for the data associated with first-order regularization. The relative changes in the output residual norms for $\lambda = 10^{-4}, 10^{-5}$ in Table 1 and $\lambda = 10^{-3}, 10^{-4}$ in Table 2 are both clearly less than 5%. Thus, the regularization parameter corresponding to the latter (or equivalently the largest) norm is chosen in accordance with the advocated criterion given in Section 4. Note also that the solution error norm is relatively stable in both cases. For zeroth-order regularization, the input estimation computed with $\lambda = 10^{-4}$ corresponds to the smallest solution error norm. This is not the case for the chosen regularization parameter of $\lambda = 10^{-3}$ for first-order regularization. However, it is clear from Tables 1 and 2 that even no regularization, i.e. $\boldsymbol{u}^{\text{NE}} = \boldsymbol{u}^{\text{LS}}$, yields satisfactory results regarding the solution error norm. This is due to the moderate level of noise added to the output and the small condition number of $\overline{\boldsymbol{H}}_0$.

In the second example in this section, the level of noise is increased $\epsilon_{\text{noise}} = 10^{-1}$ to illustrate typical effects of Eq. (11). The results corresponding to zeroth-order Tikhonov regularization are given in Table 3. The relative change between the output residual norm for $\lambda = 10^{-2}, 10^{-3}$ is less than ϵ_{tol} yielding $\lambda = 10^{-2}$ as the chosen level of regularization. The input estimation is depicted in Fig. 3. Since the level of noise was increased by a factor of 100 the solution error norm also increases by approximately 100, compare Tables 1 and 3. This is a direct consequence of perturbation errors associated with Eq. (11). The results for first-order Tikhonov regularization are given in Table 4 with the input estimation for the chosen regularization parameter depicted in Fig. 4. A drift by the estimated input from the true input is clearly visible. A slight drift was also present in the previous example with the lower degree

of noise. The reason for this behavior is that first-order regularization penalizes the derivative of the solution. Thus, a slight drift is permitted contrary to zeroth-order regularization, which penalizes the magnitude of a drifting solution. Note also that the smallest solution error norm is given for $\lambda = 10$ but the output residual norm is markedly higher for this level of regularization. However, it is believed that the chosen regularization parameter $\lambda = 10^{-1}$ yields a satisfactory balance between a small output residual norm and a small solution error norm. Moreover, the L shape of the L-curve (not shown) was found to be only vaguely visible for the data given in Table 4. The data given in Tables 1–3 do not produce L shaped curves at all. But as illustrated by these examples, it is still often possible to establish a regularization parameter that improves the estimated input. In conclusion, zeroth-order regularization produced the best input estimations for both levels of noise, and the advocated criterion for choosing the level of regularization was most accurate in this case.

Table 1: *Data for collocated case with* $\epsilon_{\text{noise}} = 10^{-3}$*. The input estimation* $\boldsymbol{u}^{\text{NE}}$ *is given by Eq. (15) with* $\boldsymbol{L}_i = \boldsymbol{L}_0$*. The asterisk marks the chosen level of regularization.*

λ	$\|\overline{\boldsymbol{H}}_0\boldsymbol{u}^{\text{NE}} - \hat{\boldsymbol{y}}^0\|_2$	$\|\boldsymbol{u}^{\text{NE}}\|_2$	$\|\boldsymbol{u}^{\text{NE}} - \hat{\boldsymbol{u}}\|_2$
10	11.4	3.32	$7.1 \cdot 10^{-1}$
1	3.32	6.61	$3.5 \cdot 10^{-1}$
10^{-1}	$5.8 \cdot 10^{-1}$	8.21	$1.0 \cdot 10^{-1}$
10^{-2}	$7.2 \cdot 10^{-2}$	8.60	$1.7 \cdot 10^{-2}$
10^{-3}	$8.6 \cdot 10^{-3}$	8.65	$2.6 \cdot 10^{-3}$
$*10^{-4}$	$4.2 \cdot 10^{-3}$	8.66	$2.4 \cdot 10^{-3}$
10^{-5}	$4.2 \cdot 10^{-3}$	8.66	$7.0 \cdot 10^{-3}$
10^{-6}	$4.2 \cdot 10^{-3}$	8.66	$8.8 \cdot 10^{-3}$
0	$4.2 \cdot 10^{-3}$	8.66	$9.0 \cdot 10^{-3}$

Table 2: *Data for collocated case with* $\epsilon_{\text{noise}} = 10^{-3}$*. The input estimation* $\boldsymbol{u}^{\text{NE}}$ *is given by Eq. (15) with* $\boldsymbol{L}_i = \boldsymbol{L}_1$*. The asterisk marks the chosen level of regularization.*

λ	$\|\overline{\boldsymbol{H}}_0\boldsymbol{u}^{\text{NE}} - \hat{\boldsymbol{y}}^0\|_2$	$\|\boldsymbol{L}_1\boldsymbol{u}^{\text{NE}}\|_2$	$\|\boldsymbol{u}^{\text{NE}} - \hat{\boldsymbol{u}}\|_2$
10	1.57	1.47	$2.7 \cdot 10^{-1}$
1	$2.2 \cdot 10^{-1}$	1.63	$6.9 \cdot 10^{-2}$
10^{-1}	$2.4 \cdot 10^{-2}$	1.66	$1.5 \cdot 10^{-2}$
10^{-2}	$4.86 \cdot 10^{-2}$	1.66	$9.6 \cdot 10^{-3}$
$*10^{-3}$	$4.2 \cdot 10^{-3}$	1.66	$9.1 \cdot 10^{-3}$
10^{-4}	$4.2 \cdot 10^{-3}$	1.66	$9.0 \cdot 10^{-3}$
10^{-6}	$4.2 \cdot 10^{-3}$	1.66	$9.0 \cdot 10^{-3}$
0	$4.2 \cdot 10^{-3}$	1.66	$9.0 \cdot 10^{-3}$

Table 3: *Data for collocated case with* $\epsilon_{\text{noise}} = 10^{-1}$. *The input estimation* $\boldsymbol{u}^{\text{NE}}$ *is given by Eq. (15) with* $\boldsymbol{L}_i = \boldsymbol{L}_0$. *The asterisk marks the chosen level of regularization.*

λ	$\|\overline{\boldsymbol{H}}_0\boldsymbol{u}^{\text{NE}} - \hat{\boldsymbol{y}}^0\|_2$	$\|\boldsymbol{u}^{\text{NE}}\|_2$	$\|\boldsymbol{u}^{\text{NE}} - \hat{\boldsymbol{u}}\|_2$
1	3.4	6.6	$3.4 \cdot 10^{-1}$
10^{-1}	$7.3 \cdot 10^{-1}$	8.2	$1.1 \cdot 10^{-1}$
$*10^{-2}$	$4.3 \cdot 10^{-1}$	8.6	$6.7 \cdot 10^{-2}$
10^{-3}	$4.2 \cdot 10^{-1}$	8.7	$1.1 \cdot 10^{-1}$
10^{-6}	$4.2 \cdot 10^{-1}$	11.5	$8.8 \cdot 10^{-1}$
0	$4.2 \cdot 10^{-1}$	11.7	$9.0 \cdot 10^{-1}$

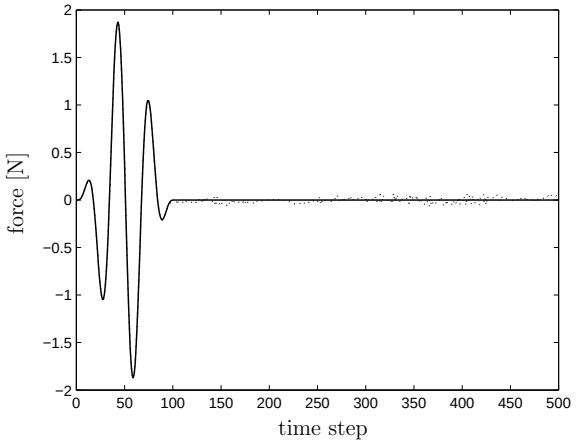

Figure 3: Input estimation for collocated case with $\epsilon_{\text{noise}} = 10^{-1}$. Estimation by method of normal equations and zeroth-order Tikhonov regularization $\lambda = 10^{-2}$.
••: $\boldsymbol{u}^{\text{NE}}$ estimation, —: $\hat{\boldsymbol{u}}$ true excitation.

Table 4: *Data for collocated case with* $\epsilon_{\text{noise}} = 10^{-1}$. *The input estimation* $\boldsymbol{u}^{\text{NE}}$ *is given by Eq. (15) with* $\boldsymbol{L}_i = \boldsymbol{L}_1$. *The asterisk marks the chosen level of regularization.*

λ	$\|\overline{\boldsymbol{H}}_0\boldsymbol{u}^{\text{NE}} - \hat{\boldsymbol{y}}^0\|_2$	$\|\boldsymbol{L}_1\boldsymbol{u}^{\text{NE}}\|_2$	$\|\boldsymbol{u}^{\text{NE}} - \hat{\boldsymbol{u}}\|_2$
10	1.7	1.4	$3.0 \cdot 10^{-1}$
1	$5.6 \cdot 10^{-1}$	1.7	$5.9 \cdot 10^{-1}$
$*10^{-1}$	$4.3 \cdot 10^{-1}$	1.7	$8.6 \cdot 10^{-1}$
10^{-2}	$4.2 \cdot 10^{-1}$	1.8	$8.9 \cdot 10^{-1}$
10^{-3}	$4.2 \cdot 10^{-1}$	1.8	$9.0 \cdot 10^{-1}$
10^{-6}	$4.2 \cdot 10^{-1}$	1.8	$9.0 \cdot 10^{-1}$
0	$4.2 \cdot 10^{-1}$	1.8	$9.0 \cdot 10^{-1}$

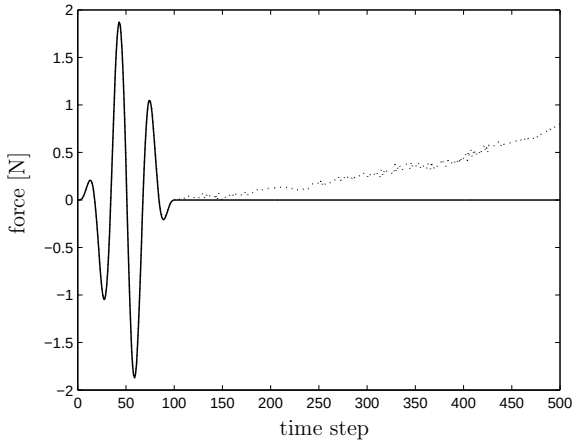

Figure 4: Input estimation for collocated case with $\epsilon_{\text{noise}} = 10^{-1}$. Estimation by method of normal equations and first-order Tikhonov regularization $\lambda = 10^{-1}$.
••: $\boldsymbol{u}^{\text{NE}}$ estimation, —: $\hat{\boldsymbol{u}}$ true excitation.

5.3 Non-collocated input/output configuration

The input estimation problem with a non-collocated input/output configuration is of greater practical importance since the desired input is in general considered inaccessible for direct measurement. This section illustrates how the advocated criterion for choosing the regularization (or truncation) parameter performs when L-curves are present. The main focus is on interpretation of the data used to construct L-curves for the different methods given in Section 3. Lastly, the special case of $\epsilon_{\text{noise}} = 0$ is treated. This case leads to a slight modification of the advocated L-curve criterion.

Consider a case where two accelerometers y_9, y_{15} are attached to masses m_9 and m_{15}, which is an example of a non-collocated input/output configuration. With the input applied to mass m_6, this input/output configuration yields a rank deficient coefficient matrix $\overline{\boldsymbol{H}}_0$, i.e. an ill-posed problem. In the following first set of numerical examples, the moderate level of output noise $\epsilon_{\text{noise}} = 10^{-3}$ is added to the unperturbed output according to Eq. (42). Moreover, the tolerance ϵ_{tol} between two consecutive output residual norms is again chosen as $\epsilon_{\text{tol}} = 0.05$. Tables 5–7 are constructed by utilizing Eq. (15), (22) and (33) with $\boldsymbol{L}_i = \boldsymbol{L}_0$, i.e. zeroth-order Tikhonov regularization, for a decreasing regularization parameter. The corresponding L-curves are given in Fig. 5. For all three methods the plateau of the output residual norm is reached for $\lambda = 10^{-4}$. The relative change in the output residual norm for $\lambda = 10^{-4}, 10^{-5}$ in Table 5 is less than 5%. It is evident from Tables 5–7 that all three methods produce equivalent solutions for $\lambda \geq 10^{-4}$, cf also Fig. 5. This is expected since they are all mathematically equivalent. Thus, $\lambda = 10^{-4}$ is chosen as the level of regularization for all three methods. Among the evaluated levels of regularization in Tables 5–7, $\lambda = 10^{-4}$ also irrefutably produces the smallest solution error norm.

As stated earlier, all three methods are mathematically equivalent. However, it is clear from Tables 5–7 or Fig. 5 that they are not numerically equivalent. The method based on block QR factorization experiences severe numerical difficulties in the transition from $\lambda = 10^{-4}$ to $\lambda = 10^{-5}$, e.g. cf Fig. 5. The reason for this unstable behavior is due to loss of orthogonality in the computed block columns of $\overline{\boldsymbol{Q}}$, as discussed in Section 3.2. However, the distinct change: compare $\lambda = 0.2 \cdot 10^{-4}$ and $\lambda = 0.15 \cdot 10^{-4}$ in Table 7, in the monitored quantities is unexpected. This phenomenon perplexes the authors, but roundoff errors together with severe cancellation effects are considered the most probable causes. A keen eye sees that the numerical deficiencies begin already for $\lambda = 0.5 \cdot 10^{-5}$, i.e. compare the solution error norm with the one given for $\lambda = 10^{-5}$ in Table 5. But this would pass unnoticed in a practical situation since this quantity would be unknown. Furthermore, it has been observed that the sensitivity is reduced for a reduced number of time steps N. The solution given by the methods of normal equations $\boldsymbol{u}^{\text{NE}}$ also looses accuracy but for a much lower level of regularization than that of $\boldsymbol{u}^{\text{BQR}}$, cf Fig. 5. The numerical deficiencies appear for $\lambda < 10^{-10}$, see Fig. 5 and cf also Table 5. The reason for this is quite different in this case. As the level of

Table 5: *Data for non-collocated case with $\epsilon_{\text{noise}} = 10^{-3}$. The input estimation $\boldsymbol{u}^{\text{NE}}$ is given by Eq. (15) with $\boldsymbol{L}_i = \boldsymbol{L}_0$. The asterisk marks the chosen level of regularization.*

λ	$\|\overline{\boldsymbol{H}}_0\boldsymbol{u}^{\text{NE}} - \hat{\boldsymbol{y}}^0\|_2$	$\|\boldsymbol{u}^{\text{NE}}\|_2$	$\|\boldsymbol{u}^{\text{NE}} - \hat{\boldsymbol{u}}\|_2$
10	11.6	3.0	$7.2 \cdot 10^{-1}$
1	3.37	6.6	$3.4 \cdot 10^{-1}$
10^{-1}	$5.7 \cdot 10^{-1}$	8.2	$1.1 \cdot 10^{-1}$
10^{-2}	$7.3 \cdot 10^{-2}$	8.6	$2.2 \cdot 10^{-2}$
10^{-3}	$9.7 \cdot 10^{-3}$	8.6	$4.4 \cdot 10^{-3}$
$*10^{-4}$	$5.8 \cdot 10^{-3}$	8.6	$3.6 \cdot 10^{-3}$
10^{-5}	$5.7 \cdot 10^{-3}$	8.7	$1.4 \cdot 10^{-2}$
10^{-6}	$5.7 \cdot 10^{-3}$	8.7	$5.1 \cdot 10^{-2}$
10^{-7}	$5.6 \cdot 10^{-3}$	8.8	$2.0 \cdot 10^{-1}$
10^{-8}	$5.6 \cdot 10^{-3}$	11	$7.8 \cdot 10^{-1}$
10^{-9}	$5.4 \cdot 10^{-3}$	26	2.8
10^{-10}	$5.3 \cdot 10^{-3}$	85	9.7
10^{-11}	$2.0 \cdot 10^{-2}$	270	31
10^{-12}	$7.4 \cdot 10^{-1}$	893	103

Table 6: *Data for non-collocated case with $\epsilon_{\text{noise}} = 10^{-3}$. The input estimation $\boldsymbol{u}^{\text{QR}}$ is given by Eq. (22) with $\boldsymbol{L}_i = \boldsymbol{L}_0$. For $\lambda > 10^{-10}$, cf Table 5.*

λ	$\|\overline{\boldsymbol{H}}_0\boldsymbol{u}^{\text{QR}} - \hat{\boldsymbol{y}}^0\|_2$	$\|\boldsymbol{u}^{\text{QR}}\|_2$	$\|\boldsymbol{u}^{\text{QR}} - \hat{\boldsymbol{u}}\|_2$
$\vdots$			
10^{-10}	$5.3 \cdot 10^{-3}$	85	9.7
10^{-11}	$5.2 \cdot 10^{-3}$	270	31
10^{-12}	$4.9 \cdot 10^{-3}$	893	103

Table 7: *Data for non-collocated case with $\epsilon_{\text{noise}} = 10^{-3}$. The input estimation $\boldsymbol{u}^{\text{BQR}}$ is given by Eq. (33) with $\boldsymbol{L}_i = \boldsymbol{L}_0$. The asterisk marks the chosen level of regularization. For $\lambda > 10^{-4}$, cf Table 5.*

λ	$\|\overline{\boldsymbol{H}}_0\boldsymbol{u}^{\text{BQR}} - \hat{\boldsymbol{y}}^0\|_2$	$\|\boldsymbol{u}^{\text{BQR}}\|_2$	$\|\boldsymbol{u}^{\text{BQR}} - \hat{\boldsymbol{u}}\|_2$
$\vdots$			
$*10^{-4}$	$5.8 \cdot 10^{-3}$	8.6	$3.6 \cdot 10^{-3}$
$0.5 \cdot 10^{-4}$	$5.8 \cdot 10^{-3}$	9.2	$3.5 \cdot 10^{-1}$
$0.25 \cdot 10^{-4}$	$5.8 \cdot 10^{-3}$	9.6	$4.7 \cdot 10^{-1}$
$0.2 \cdot 10^{-4}$	$5.8 \cdot 10^{-3}$	9.7	$5.0 \cdot 10^{-1}$
$0.15 \cdot 10^{-4}$	72	$2.1 \cdot 10^{4}$	$2.5 \cdot 10^{3}$
10^{-5}	45	$1.7 \cdot 10^{4}$	$1.9 \cdot 10^{3}$

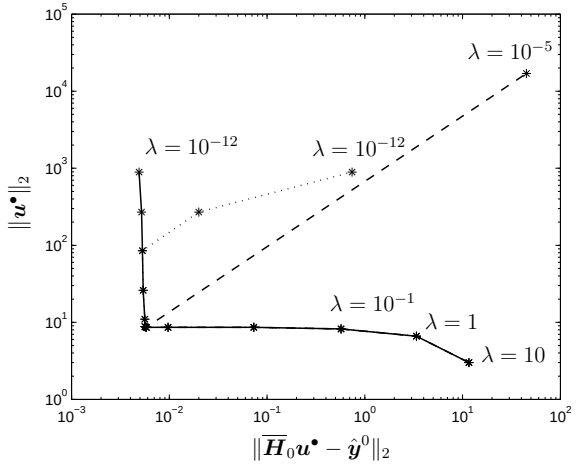

Figure 5: L-curve for non-collocated case with $\epsilon_{\text{noise}} = 10^{-3}$ and $\boldsymbol{L}_i = \boldsymbol{L}_0$. λ is the level of Tikhonov regularization. $\cdots$: $\boldsymbol{u}^{\text{NE}}$, – –: $\boldsymbol{u}^{\text{BQR}}$, —: $\boldsymbol{u}^{\text{QR}}$.

regularization λ decreases the condition number of the modified coefficient matrix increases. The condition number in square affects the computation of $\boldsymbol{u}^{\text{NE}}$, which is not the case for $\boldsymbol{u}^{\text{QR}}$. Thus, $\boldsymbol{u}^{\text{NE}}$ will loose accuracy for a smaller condition number than that of $\boldsymbol{u}^{\text{QR}}$. However, as the level of regularization approaches $\epsilon_{\text{mach}} \approx 10^{-16}$ the computation of $\boldsymbol{u}^{\text{QR}}$ will also eventually become inaccurate.

The results corresponding to $\boldsymbol{u}^{\text{TSVD}}$, cf Eq. (40), are given in Table 8. Figure 6 depicts the associated L-curve. In Table 8, the truncation parameter is consecutively increased by adding 10 singular values close to the plateau. For $k = 70, 80$ the relative difference in the output residual norm is less than 5%, thus $k = 70$ is chosen as the level of truncation. This level corresponds to the smallest solution error norm, cf Table 8, but it is also clear that $k = 60$ or $k = 80$ yield excellent estimates of the sought input. By comparing the L-curve given in Fig. 6 with the L-curve corresponding to the results of $\boldsymbol{u}^{\text{QR}}$ in Fig. 5, it can bee seen that these solutions are closely related, which is discussed in Section 3.4. The two solutions perform approximately equally well considering numerical accuracy.

Table 8: *Data for non-collocated case with $\epsilon_{\text{noise}} = 10^{-3}$. The input estimation $\boldsymbol{u}^{\text{TSVD}}$ is given by Eq. (40). The asterisk marks the chosen level of truncation.*

k	$\|\overline{\boldsymbol{H}}_0\boldsymbol{u}^{\text{TSVD}} - \hat{\boldsymbol{y}}^0\|_2$	$\|\boldsymbol{u}^{\text{TSVD}}\|_2$	$\|\boldsymbol{u}^{\text{TSVD}} - \hat{\boldsymbol{u}}\|_2$
10	14	4.2	$8.7 \cdot 10^{-1}$
30	$5.1 \cdot 10^{-1}$	8.5	$1.8 \cdot 10^{-1}$
50	$2.0 \cdot 10^{-2}$	8.7	$1.9 \cdot 10^{-2}$
60	$6.1 \cdot 10^{-3}$	8.7	$6.1 \cdot 10^{-3}$
$*70$	$5.8 \cdot 10^{-3}$	8.7	$2.4 \cdot 10^{-3}$
80	$5.8 \cdot 10^{-3}$	8.7	$9.2 \cdot 10^{-3}$
100	$5.7 \cdot 10^{-3}$	8.7	$8.4 \cdot 10^{-2}$
120	$5.7 \cdot 10^{-3}$	9.5	$4.3 \cdot 10^{-1}$
160	$5.5 \cdot 10^{-3}$	35	3.9
200	$5.3 \cdot 10^{-3}$	149	17

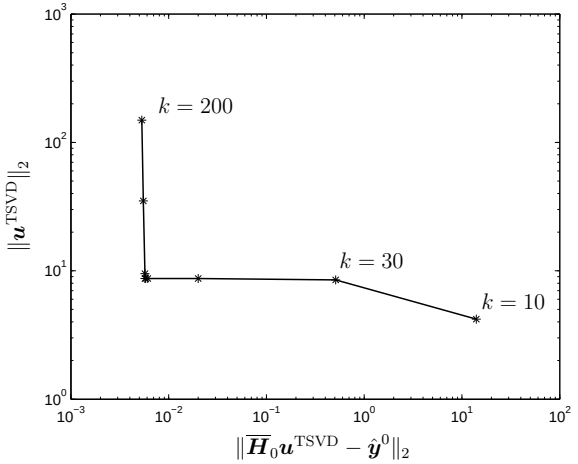

Figure 6: L-curve for non-collocated case with $\epsilon_{\text{noise}} = 10^{-3}$. k is the number of terms in the truncated SVD.

Tables 9 and 10 give the results corresponding to $\boldsymbol{u}^{\mathrm{NE}}$ and $\boldsymbol{u}^{\mathrm{QR}}$, which are given by Eqs. (15) and (22), respectively, with first-order Tikhonov regularization. The numerical behavior of both methods for small levels of regularization $\lambda < 10^{-10}$ is similar to that of the results for zeroth-order regularization, compare Figs. 5 and 7. As seen in Fig. 7, the output residual norm for $\boldsymbol{u}^{\mathrm{NE}}$ diverges from the output residual norm for $\boldsymbol{u}^{\mathrm{QR}}$. This is due to the effectively larger condition number of the modified coefficient matrix given by the method of normal equations. The level of regularization is chosen as $\lambda = 10^{-3}$ in accordance with the advocated L-curve criterion, but a smaller input solution error norm is produced for $\lambda = 10^{-2}$. However, both levels of regularization yield satisfactory results, cf Table 9. It should also be stressed that the solution error norms computed for zeroth-order and first-order Tikhonov regularization are of the same order of magnitude for the chosen level of regularization in each case, compare Tables 5 and 9. The results corresponding to $\boldsymbol{u}^{\mathrm{BQR}}$ with $\boldsymbol{L}_i = \boldsymbol{L}_1$ are omitted due to the numerical deficiencies encountered for $\boldsymbol{L}_i = \boldsymbol{L}_0$, cf Fig. 5.

Table 9: *Data for non-collocated case with $\epsilon_{\mathrm{noise}} = 10^{-3}$. The input estimation $\boldsymbol{u}^{\mathrm{NE}}$ is given by Eq. (15) with $\boldsymbol{L}_i = \boldsymbol{L}_1$. The asterisk marks the chosen level of regularization.*

λ	$\|\overline{\boldsymbol{H}}_0\boldsymbol{u}^{\mathrm{NE}} - \hat{\boldsymbol{y}}^0\|_2$	$\|\boldsymbol{L}_1\boldsymbol{u}^{\mathrm{NE}}\|_2$	$\|\boldsymbol{u}^{\mathrm{NE}} - \hat{\boldsymbol{u}}\|_2$
10	1.57	1.4	$3.1 \cdot 10^{-1}$
1	$2.1 \cdot 10^{-1}$	1.6	$1.1 \cdot 10^{-1}$
10^{-1}	$2.4 \cdot 10^{-2}$	1.7	$1.1 \cdot 10^{-2}$
10^{-2}	$6.3 \cdot 10^{-3}$	1.7	$3.6 \cdot 10^{-3}$
$*10^{-3}$	$5.8 \cdot 10^{-3}$	1.7	$4.1 \cdot 10^{-3}$
10^{-4}	$5.8 \cdot 10^{-3}$	1.7	$8.3 \cdot 10^{-3}$
10^{-5}	$5.8 \cdot 10^{-3}$	1.7	$2.6 \cdot 10^{-2}$
10^{-6}	$5.7 \cdot 10^{-3}$	1.7	$8.0 \cdot 10^{-2}$
10^{-7}	$5.6 \cdot 10^{-3}$	2.5	$2.8 \cdot 10^{-1}$
10^{-8}	$5.5 \cdot 10^{-3}$	6.6	$9.0 \cdot 10^{-1}$
10^{-9}	$5.4 \cdot 10^{-3}$	23	2.8
10^{-10}	$5.3 \cdot 10^{-3}$	79	8.5
10^{-11}	$1.0 \cdot 10^{-2}$	253	24
10^{-12}	$5.8 \cdot 10^{-2}$	828	68

Table 10: *Data for non-collocated case with $\epsilon_{\mathrm{noise}} = 10^{-3}$. The input estimation $\boldsymbol{u}^{\mathrm{QR}}$ is given by Eq. (22) with $\boldsymbol{L}_i = \boldsymbol{L}_1$. For $\lambda > 10^{-10}$, cf Table 9.*

λ	$\|\overline{\boldsymbol{H}}_0\boldsymbol{u}^{\mathrm{QR}} - \hat{\boldsymbol{y}}^0\|_2$	$\|\boldsymbol{L}_1\boldsymbol{u}^{\mathrm{QR}}\|_2$	$\|\boldsymbol{u}^{\mathrm{QR}} - \hat{\boldsymbol{u}}\|_2$
$\vdots$			
10^{-10}	$5.3 \cdot 10^{-3}$	79	8.5
10^{-11}	$5.2 \cdot 10^{-3}$	253	24
10^{-12}	$5.0 \cdot 10^{-3}$	828	68

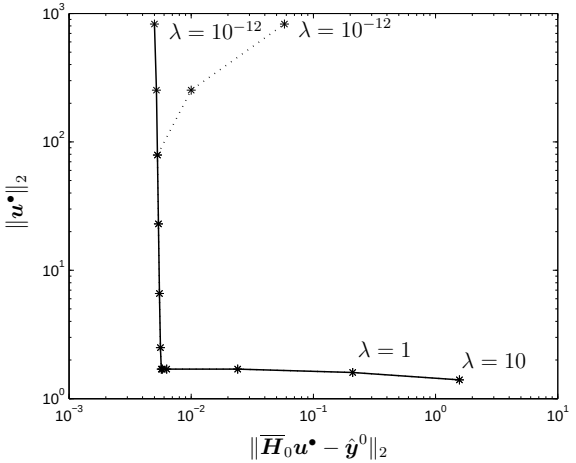

Figure 7: L-curve for non-collocated case with $\epsilon_{\mathrm{noise}} = 10^{-3}$ and $\boldsymbol{L}_i = \boldsymbol{L}_1$. λ is the level of Tikhonov regularization. ⋯: $\boldsymbol{u}^{\mathrm{NE}}$, —: $\boldsymbol{u}^{\mathrm{QR}}$.

As a last example, the special case of noise free measurements is investigated, i.e. $\epsilon_{\text{noise}} = 0$. When $\epsilon_{\text{noise}} \to 0$, the plateau of the output residual norm converges to a distinct and well localized minimum. Thus, the advocated L-curve criterion is modified in choosing the regularization (or truncation) parameter rendering this minimal norm. The output residual norms corresponding to the solutions $\boldsymbol{u}^{\text{BQR}}$, $\boldsymbol{u}^{\text{NE}}$ and $\boldsymbol{u}^{\text{QR}}$ with zeroth-order Tikhonov regularization are plotted in Fig. 8 versus the regularization parameter, cf also Tables 11 and 12 given in Appendix A. As in the previous example, the block QR factorization algorithm fails drastically between $\lambda = 10^{-4}$ and $\lambda = 10^{-5}$. The minimum of the output residual norm is obtained for $\lambda = 10^{-4}$ with a solution error norm of $1.6 \cdot 10^{-3}$. For $\boldsymbol{u}^{\text{NE}}$, the minimal output residual norm is attained for $\lambda = 10^{-7}$ but the minimum of the solution error norm corresponds to $\lambda = 10^{-9}$, cf Table 11. Even better results are produced by $\boldsymbol{u}^{\text{QR}}$, cf Table 12. Here, the chosen level of regularization $\lambda = 10^{-12}$ also coincides with the smallest solution error norm. The truncated SVD solution $\boldsymbol{u}^{\text{TSVD}}$ yields an output and a solution error norm similar to that of $\boldsymbol{u}^{\text{QR}}$ for the chosen level of truncation $k = 240$, cf Fig. 9 and Table 13 in Appendix A. However, the smallest solution error norm is given for $k = 498$ which is equal to the numerical rank of $\overline{\boldsymbol{H}}_0$. This choice would be difficult to motivate in practice, since the output residual norm is larger in this case. As k increases so does the condition number of the modified coefficient matrix, the direct consequence of which is seen for $k > 240$ in Table 13. The algorithm based on QR factorization with column

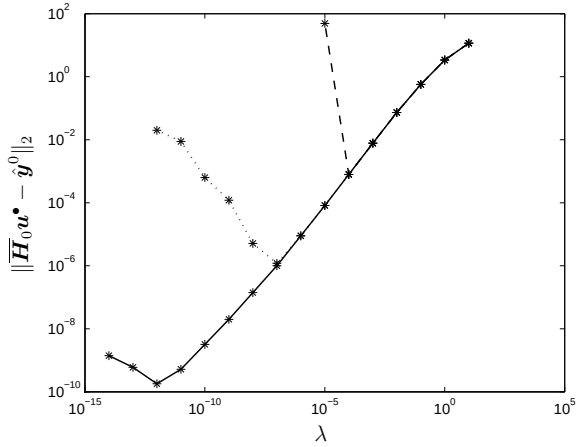

Figure 8: Output residual norm for non-collocated case with $\epsilon_{\text{noise}} = 0$ and $\boldsymbol{L}_i = \boldsymbol{L}_0$. $\cdots$: $\boldsymbol{u}^{\text{NE}}$, – –: $\boldsymbol{u}^{\text{BQR}}$, —: $\boldsymbol{u}^{\text{QR}}$.

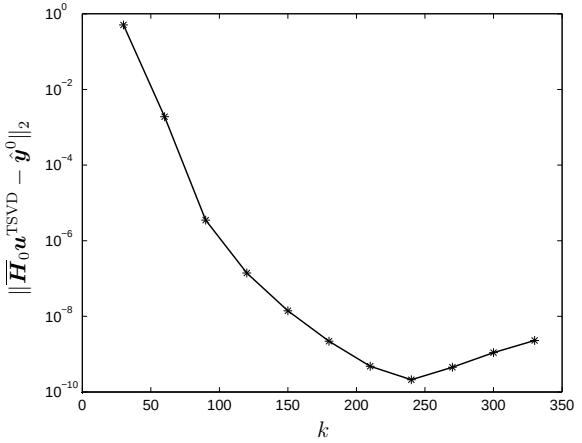

Figure 9: Output residual norm for non-collocated case with $\epsilon_{\text{noise}} = 0$.

pivoting, see Section 3.3, also successfully identifies the numerical rank of $\overline{\boldsymbol{H}}_0$ as 498. Thus, $\boldsymbol{R}_{11} \in \mathbb{R}^{498\times 498}$ in Eq. (35). The output residual norm corresponding to $\boldsymbol{u}^{\text{B}}$ is a striking $8.2 \cdot 10^{-14}$ with a solution error norm of $7.8 \cdot 10^{-8}$. It should nonetheless be noted that in this special case, with $\epsilon_{\text{noise}} = 0$, it is possible to satisfy all the equations of the output residual norm in theory, i.e. $\|\overline{\boldsymbol{H}}_0\boldsymbol{u} - \hat{\boldsymbol{y}}^0\|_2 = \boldsymbol{0}$. This is generally not the case for $\epsilon_{\text{noise}} > 0$.

6 CONCLUSIONS

Four principally different methods of solving input estimation problems in structural mechanics have been studied. One of the methods is specifically derived to take account of the upper block triangular Toeplitz matrix structure associated with input estimation problems. All of the methods are based on an enlarged damped least squares formulation of the corresponding input estimation problem, cf Eq. (13). An advocated criterion for choosing an appropriate level of regularization has been introduced and assessed numerically for the different methods. It is based on the data used to construct L-curves but it has the advantage of being defined even when the L-curves are not present, as is usually the case for the collocated input/output configuration. In this case, perturbation errors associated with Eq. (11) are reduced. The main focus has been to describe and interpret numerical aspects of the different methods from an L-curve point of view. An extensive set of numerical examples are used in an attempt

to support the numerical argumentation. In conclusion, the advocated criterion seems to be most effective for the methods associated with zeroth-order Tikhonov regularization.

7 ACKNOWLEDGEMENTS

Financial support was given by Volvo Car Corporation and VINNOVA within its Swedish National Road Vehicle Program. Patrik expresses his gratitude to Prof. Thomas Abrahamsson at the Department of Applied Mechanics, Chalmers University of Technology, and Dr. Mikael Fermér at Volvo Car Corporation for their support and encouragement.

REFERENCES

[1] K. K. Stevens. Force identification problems - an overview. *Proceedings of SEM Spring Meeting, Houston*, pages 838–844, 1987.

[2] B. J. Dobson and E. Rider. A review of the indirect calculations of excitation forces from measured strucural response data. *Proceedings of the Institution of Mechanical Engineers Part C: Journal of Mechanical Engineering Science*, C2:204:69–75, 1990.

[3] L. J. L. Nordström and T. P. Nordberg. A critical comparison of time domain load identification methods. *Proceedings of the Sixth International Conference on Motion and Vibration Control*, 2:1151–1156, 2002.

[4] A. D. Steltzner, D. C. Kammer, and P. Milenkovic. A time domain method for estimating forces applied to an unrestrained structure. *Journal of Vibration and Acoustics*, 123:524–532, 2001.

[5] T. G. Carne, V. I. Bateman, and R. L. Mayes. Force reconstruction using a sum of weighted accelerations technique. *Proceedings of the 10th International Modal Analysis Conference*, pages 291–298, 1992.

[6] T. P. Nordberg. An iterative approach to road/profile identification utilizing wavelet parameterization. *To Appear in Vehicle System Dynamics*, 2004.

[7] P. K. Lamm. Inverse problems and ill-posedness. *Inverse Problems in Engineering: Theory and Practice ASME 1993*, pages 1–10, 1993.

[8] D. L. Phillips. A technique for the numerical solution of certain equations of the first kind. *J. ACM*, 9:84–97, 1962.

[9] A. N. Tikhonov. Solution of incorrectly formulated problems and the regularization method. *Soviet Math. Dokl.*, 4:1035–1038, 1963.

[10] A. N. Tikhonov and Y. Arsenin. *Solution of Ill-posed Problems*. Wiley, 1977.

[11] P. C. Hansen. Analysis of discrete ill-posed problems by means of the L-curve. *SIAM Review*, 34:561–580, 1992.

[12] P. K. Lamm and L. Eldén. Numerical solution of first-kind Volterra equations by sequential Tikhonov regularization. *SIAM J. Numer. Anal.*, 34(4):1432–1450, 1997.

[13] T. P. Nordberg and I. Gustafsson. Dynamic regularization of input estimation problems by explicit block inversion. *Submitted for International Publication*, 2004.

[14] G. H. Golub and C. F. van Loan. *Matrix Computations*. The John Hopkins University Press, third edition, 1996.

[15] L. Eldén. An efficient algorithm for the regularization of ill-conditioned least squares problems with triangular Toeplitz matrix. *SIAM J. Sci. Statist. Comput.*, 5:229–236, 1984.

[16] P. C. Hansen. Deconvolution and regularization with Toeplitz matrices. *Numerical Algorithms*, 29:323–378, 2002.

[17] Å. Björck. *Numerical Methods for Least Squares Problems*. SIAM, Philadelphia, 1996.

[18] T. Kailath. *Linear Systems*. Prentice Hall PTR, Upper Saddle River, New Jersey, 1980.

[19] Å. Björck and L. Eldén. *Methods in Numerical Algebra for Ill-posed Problems*. Report LiTH–MAT–R–1979–33, Department of Mathematics, Linköping University, Sweden, 1979.

[20] M. T. Heath. *Scientific Computing: An Introductory Survey*. The McGraw-Hill Companies, Inc., 1997.

[21] L. J. L. Nordström and T. P. Nordberg. A time delay method to solve non-collocated input estimation problems. *To Appear in Mechanical Systems and Signal Processing*, 18:1469–1483, 2004.

[22] M. K. Sain and J. L. Massey. Invertibility of linear time-invariant dynamical system. *IEEE Transactions on Automatic Control*, 14(2):141–149, 1969.

[23] L. M. Silverman. Inversion of multivariable linear systems. *IEEE Transactions on Automatic Control*, 14(3):270–276, 1969.

Appendix A: Complementary tables

Table 11: *Data for non-collocated case with* $\epsilon_{\text{noise}} = 0$. *The input estimation* $\boldsymbol{u}^{\text{NE}}$ *is given by Eq. (15) with* $\boldsymbol{L}_i = \boldsymbol{L}_0$. *The asterisk marks the chosen level of regularization, cf also Fig. 8.*

λ	$\|\overline{\boldsymbol{H}}_0\boldsymbol{u}^{\text{NE}} - \hat{\boldsymbol{y}}^0\|_2$	$\|\boldsymbol{u}^{\text{NE}}\|_2$	$\|\boldsymbol{u}^{\text{NE}} - \hat{\boldsymbol{u}}\|_2$
10	11.6	3.0	$7.2 \cdot 10^{-1}$
1	3.4	6.6	$3.4 \cdot 10^{-1}$
10^{-1}	$5.7 \cdot 10^{-1}$	8.2	$1.1 \cdot 10^{-1}$
10^{-2}	$7.3 \cdot 10^{-2}$	8.6	$2.2 \cdot 10^{-2}$
10^{-3}	$7.8 \cdot 10^{-3}$	8.7	$4.3 \cdot 10^{-3}$
10^{-4}	$7.9 \cdot 10^{-4}$	8.7	$1.6 \cdot 10^{-3}$
10^{-5}	$8.2 \cdot 10^{-5}$	8.7	$8.1 \cdot 10^{-4}$
10^{-6}	$8.9 \cdot 10^{-6}$	8.7	$4.1 \cdot 10^{-4}$
$*10^{-7}$	$1.2 \cdot 10^{-6}$	8.7	$2.2 \cdot 10^{-4}$
10^{-8}	$5.1 \cdot 10^{-6}$	8.7	$1.1 \cdot 10^{-4}$
10^{-9}	$1.2 \cdot 10^{-4}$	8.7	$6.2 \cdot 10^{-5}$
10^{-10}	$6.3 \cdot 10^{-4}$	8.7	$1.2 \cdot 10^{-4}$
10^{-11}	$8.8 \cdot 10^{-3}$	8.7	$1.7 \cdot 10^{-3}$
10^{-12}	$2.0 \cdot 10^{-1}$	8.7	$3.8 \cdot 10^{-2}$

Table 12: *Data for non-collocated case with* $\epsilon_{\text{noise}} = 0$. *The input estimation* $\boldsymbol{u}^{\text{QR}}$ *is given by Eq. (22) with* $\boldsymbol{L}_i = \boldsymbol{L}_0$. *The asterisk marks the chosen level of regularization. For* $\lambda > 10^{-6}$, *cf Table 11 and also Fig. 8.*

λ	$\|\overline{\boldsymbol{H}}_0\boldsymbol{u}^{\text{QR}} - \hat{\boldsymbol{y}}^0\|_2$	$\|\boldsymbol{u}^{\text{QR}}\|_2$	$\|\boldsymbol{u}^{\text{QR}} - \hat{\boldsymbol{u}}\|_2$
$\vdots$			
10^{-6}	$8.9 \cdot 10^{-6}$	8.7	$4.1 \cdot 10^{-4}$
10^{-7}	$1.0 \cdot 10^{-6}$	8.7	$2.2 \cdot 10^{-4}$
10^{-8}	$1.4 \cdot 10^{-7}$	8.7	$1.2 \cdot 10^{-4}$
10^{-9}	$2.0 \cdot 10^{-8}$	8.7	$6.0 \cdot 10^{-5}$
10^{-10}	$3.2 \cdot 10^{-9}$	8.7	$3.2 \cdot 10^{-5}$
10^{-11}	$5.2 \cdot 10^{-10}$	8.7	$1.7 \cdot 10^{-5}$
$*10^{-12}$	$1.8 \cdot 10^{-10}$	8.7	$1.4 \cdot 10^{-5}$
10^{-13}	$6.0 \cdot 10^{-10}$	8.7	$7.4 \cdot 10^{-5}$
10^{-14}	$1.4 \cdot 10^{-9}$	8.7	$6.9 \cdot 10^{-4}$

Table 13: *Data for non-collocated case with* $\epsilon_{\text{noise}} = 0$. *The input estimation* $\boldsymbol{u}^{\text{TSVD}}$ *is given by Eq. (40). The asterisk marks the chosen level of truncation, cf also Fig. 9.*

k	$\|\overline{\boldsymbol{H}}_0\boldsymbol{u}^{\text{TSVD}} - \hat{\boldsymbol{y}}^0\|_2$	$\|\boldsymbol{u}^{\text{TSVD}}\|_2$	$\|\boldsymbol{u}^{\text{TSVD}} - \hat{\boldsymbol{u}}\|_2$
30	$5.1 \cdot 10^{-1}$	8.5	$1.8 \cdot 10^{-1}$
60	$1.9 \cdot 10^{-3}$	8.7	$6.1 \cdot 10^{-3}$
90	$3.5 \cdot 10^{-6}$	8.7	$5.3 \cdot 10^{-4}$
120	$1.4 \cdot 10^{-7}$	8.7	$1.7 \cdot 10^{-4}$
150	$1.4 \cdot 10^{-8}$	8.7	$7.4 \cdot 10^{-5}$
180	$2.2 \cdot 10^{-9}$	8.7	$3.8 \cdot 10^{-5}$
210	$4.8 \cdot 10^{-10}$	8.7	$2.2 \cdot 10^{-5}$
$*240$	$2.1 \cdot 10^{-10}$	8.7	$1.4 \cdot 10^{-5}$
270	$4.5 \cdot 10^{-10}$	8.7	$9.3 \cdot 10^{-6}$
300	$1.1 \cdot 10^{-9}$	8.7	$6.6 \cdot 10^{-6}$
330	$2.3 \cdot 10^{-9}$	8.7	$5.0 \cdot 10^{-6}$
360	$3.9 \cdot 10^{-9}$	8.7	$3.8 \cdot 10^{-6}$
390	$7.9 \cdot 10^{-9}$	8.7	$3.0 \cdot 10^{-6}$
420	$1.4 \cdot 10^{-8}$	8.7	$2.3 \cdot 10^{-6}$
450	$3.3 \cdot 10^{-8}$	8.7	$1.7 \cdot 10^{-6}$
480	$7.6 \cdot 10^{-8}$	8.7	$1.1 \cdot 10^{-6}$
498	$1.2 \cdot 10^{-7}$	8.7	$2.4 \cdot 10^{-7}$